Cerebral Cortex, December 2019;29: 5269–5284

doi: 10.1093/cercor/bhz064
Advance Access Publication Date: 8 May 2019
Original Article

ORIGINAL ARTICLE

Structural Covariance Reveals Alterations in Control and Salience Network Integrity in Chronic Schizophrenia

R. Nathan Spreng[1,2], Elizabeth DuPre[1], Jie Lisa Ji[3,4], Genevieve Yang[8], Caroline Diehl[9], John D. Murray[6], Godfrey D. Pearlson[3,5,6] and Alan Anticevic[3,4,5,7]

[1]Montreal Neurological Institute, Department of Neurology and Neurosurgery, McGill University, Montreal, QC, H3A 2B4, Canada, [2]Departments of Psychiatry and Psychology, McGill University, Montreal, QC, H3A 2B4, Canada, [3]Department of Psychiatry, Yale University School of Medicine, 300 George Street, New Haven, CT 06511, USA, [4]Interdepartmental Neuroscience Program, Yale University, New Haven, CT 06520, USA, [5]Department of Psychology, Yale University, 2 Hillhouse Avenue, CT 06520, USA, [6] Center for Neural Science, New York University, New York, NY 10003, USA, [7]Olin Neuropsychiatry Research Center, Institute of Living, Hartford Hospital, 200 Retreat Avenue, CT 06106, USA, [8]Department of Psychiatry, Mount Sinai School of Medicine, 1 Gustave L. Levy Pl, New York, NY 10029 and [9]Department of Psychology, University of California at Los Angeles, 1285 Franz Hall Box 951563 Los Angeles, CA 90095-1563

Address correspondence to Alan Anticevic Department of Psychiatry Yale University 34 Park St. New Haven, CT 06519. Email: alan.anticevic@yale.edu.

Abstract

Schizophrenia (SCZ) is recognized as a disorder of distributed brain dysconnectivity. While progress has been made delineating large-scale functional networks in SCZ, little is known about alterations in grey matter integrity of these networks. We used a multivariate approach to identify the structural covariance of the salience, default, motor, visual, fronto-parietal control, and dorsal attention networks. We derived individual scores reflecting covariance in each structural image for a given network. Seed-based multivariate analyses were conducted on structural images in a discovery (n = 90) and replication (n = 74) sample of SCZ patients and healthy controls. We first validated patterns across all networks, consistent with well-established functional connectivity reports. Next, across two SCZ samples, we found reliable and robust reductions in structural integrity of the fronto-parietal control and salience networks, but not default, dorsal attention, motor and sensory networks. Well-powered exploratory analyses failed to identify relationships with symptoms. These findings provide evidence of selective structural decline in associative networks in SCZ. Such decline may be linked with recently identified functional disturbances in associative networks, providing more sensitive multi-modal network-level probes in SCZ. Absence of symptom effects suggests that identified disturbances may underlie a trait-type marker in SCZ.

Key words: partial least squares, magnetic resonance imaging, psychosis, structural network abnormalities

Introduction

The human brain is organized into large-scale networks, which have been reliably delineated using resting-state functional connectivity MRI methods (Power et al. 2011; Yeo et al. 2011; Buckner et al. 2013). These large-scale brain systems can be characterized by examining structural covariance networks, an approach that examines inter-individual differences in regional brain volume, co-varying with other brain structures, across the population (Alexander-Bloch et al. 2013a). Across individuals, intrinsically connected functional brain networks can be topographically represented in the structural patterns of cortical grey matter, complementing functional investigations. Recent studies have successfully leveraged such approaches to define structural covariance networks across the human lifespan (DuPre and Spreng 2017), and subsequently used this topology to estimate the structural integrity of such networks from standard individual T1 anatomical images. Structural covariance analysis, as a method, largely replicates the network architecture defined using functional neuroimaging approaches, including the salience, default, motor, visual, fronto-parietal control, and dorsal attention systems (Zielinski et al. 2010; Clos et al. 2014). Such methods can provide unique insights into grey matter integrity within these networks, which could be severely impacted by neuropsychiatric illness.

Schizophrenia (SCZ) in particular is one of the most disabling neuropsychiatric conditions in the world (Murray et al. 1996) and is associated with distributed neural abnormalities. It is well established that SCZ is a disorder of distributed brain 'dysconnectivity' (Stephan et al. 2006; Cocchi et al. 2014; Ellison-Wright et al. 2014) emerging from complex biological alterations across multiple neural systems (Coyle JT 2006). Its symptoms lead to profound economic cost and lifelong disability for most patients (Murray and Lopez 1996). Therefore, characterizing neural disturbances in SCZ constitutes a critical research goal and requires the identification of both pathophysiological mechanisms and better neural markers to guide intervention and treatment. Resting-state functional connectivity approaches have revealed evidence for functional connectivity disruptions in associative fronto-parietal control networks in chronic SCZ (Baker et al. 2014), which appear to be related to abnormal blood oxygen level dependent (BOLD) signal variance across these same networks (Yang et al. 2014). Concurrently, studies have identified profound alterations in thalamo-cortical information flow (Woodward et al. 2012; Anticevic et al. 2013a; Anticevic et al. 2014) and neural systems involved in salience processing (Palaniyappan et al. 2013). These studies provide emerging support for functional disruptions in associative cortical networks in SCZ (Pearlson et al. 1996; Pearlson and Marsh 1999; Whitfield-Gabrieli et al. 2009; Cocchi et al. 2014). However, it is unclear whether SCZ is associated with altered structural integrity across these same networks. Testing this hypothesis is vital for two reasons: i) it establishes a potentially complementary neural marker that can be used in conjunction with functional measures, extending standard localization methods of voxel-based morphometric studies (Bora et al. 2011); ii) if viable, this structural network measure can lead to important re-analyses of many existing structural datasets with a measure sensitive to network-level disturbances in structural gray matter integrity.

Prior work examining structural covariance in SCZ identified altered inter-regional correlations between the frontal–temporal and frontal–parietal regions (for review, see (Alexander-Bloch et al. 2013b). Using graph analytic measures, this work showed that SCZ is associated with significantly reduced hierarchy and increased connection distance, resulting in attenuated network relationships among associative cortical areas (Bassett et al. 2008; Lynn and Bassett 2018). Structural covariance analysis has revealed alterations across cortex in primary and association regions in SCZ (Palaniyappan et al. 2015; Zugman et al. 2015; Kuang et al. 2017; Lefort-Besnard et al. 2018; Liu et al. 2018; Palaniyappan et al. 2018) with moderate convergence across studies implicating executive and salience processing regions. The goal of our study was to test the hypothesis that structural covariance methods can reveal robust and replicable network-level alterations in SCZ relative to matched controls.

We used a novel seed-based multivariate approach to identify the structural covariance of the brain's large-scale networks and to provide novel insights into grey matter differences within these networks in SCZ relative to healthy control participants. Our aim was to first isolate the structural covariance networks – that is, regions that show similar variability in gray matter volume. In turn, we sought to characterize changes to the grey matter integrity within these networks in SCZ. As noted, based on existing functional studies, we hypothesized that structural integrity disturbances would be particularly pronounced in executive/control and salience networks (Anticevic et al. 2013b; Frangou 2014). We tested this hypothesis in a large sample of chronic SCZ patients (N = 90) by: i) identifying the salience, default, motor, visual, fronto-parietal control, and dorsal attention structural covariance networks across all individuals; ii) quantifying alterations in SCZ across these systems; iii) replicating our findings using an independent large sample of chronic SCZ patients (N = 74).

Materials and Methods

Participants

We examined two independent SCZ samples: i) discovery sample: 90 chronic SCZ patients and 90 demographically matched HCS (Table 1); ii) replication sample: 71 SCZ patients and 74 demographically matched HCS obtained from a publicly-distributed dataset provided by the Center for Biomedical Research Excellence (COBRE) (http://fcon_1000..projects.nitrc.org/indi/retro/cobre.html) (Table 2). Identical recruitment and exclusion criteria were used to assess participants at both sites. Furthermore, across samples, all subjects met identical neuroimaging exclusion criteria and underwent identical preprocessing and analyses.

Discovery sample SCZ participants (N = 90) were identified through outpatient clinics and community mental health facilities in the Hartford, CT area. Complete recruitment details for this sample are described in our prior work (Anticevic et al. 2013a). Briefly, patient inclusion criteria were as follows: i) SCZ diagnosis as determined by the Structured Clinical Interview (SCID) for the Diagnostic and Statistical Manual of Mental Disorders-IV (DSM-IV) (First et al. 2002), administered by experienced MA or PhD-level research clinicians; ii) no major medical or neurological conditions (e.g. epilepsy, migraine, head trauma with loss of consciousness); and iii) IQ > 70 assessed by widely-accepted methods for estimating premorbid intelligence levels [either National Adult Reading Test (NART), Wide Range Achievement Test (WRAT) or Wechsler Test of

Table 1 Clinical and Demographic Characteristics - Discovery Sample

Characteristic	HCS (N = 90)		SCZ (N = 87)		Significance	
	M	S.D.	M	S.D.	T Value / Chi-Square	P Value (two-tailed)
Age (in years)	30.71	11.99	32.93	11.25	1.35	0.18
Gender (% male)	65.56		73.00		1.15	0.25
Father's Education (in years)	14.37	3.21	13.67	3.47	1.22	0.22
Mother's Education (in years)	13.99	2.81	13.50	2.92	0.94	0.35
Participant's education (in years)	15.24	2.22	13.18	2.21	6.03	0.00*
Handedness (% right)	88.89		80.00		0.44	0.66
IQ Estimate	106.77	8.92	97.78	15.71	4.34	0.00
Medication (CPZ equivalents)	-	-	225.43	197.31	-	-
PANSS Positive Symptoms	-	-	15.76	4.78	-	-
PANSS Negative Symptoms	-	-	14.18	5.42	-	-
PANSS General Psychopathology	-	-	30.43	7.31	-	-
PANSS Total Psychopathology	-	-	60.37	14.36	-	-

HCS, healthy comparison subjects; SCZ, patients diagnosed with schizophrenia; PANSS, Positive and Negative Syndrome Scale; M, mean; SD, standard deviation; IQ, intelligence quotient; CPZ, chlorpromazine; age, education levels, parental education, are expressed in years. CPZ equivalents were calculated according to latest validated approaches (Andreasen et al. 2010). * denotes a significant T statistic for the between-group t-test.

Table 2 Clinical and Demographic Characteristics - Replication Sample

Characteristic	HCS (N = 74)		SCZ (N = 71)		Significance	
	M	S.D.	M	S.D.	T Value / Chi-Square	P Value (two-tailed)
Age (in years)	35.82	11.58	38.14	13.99	1.09	0.28
Gender (% male)	68.92		80.28		1.57	0.12
Parental Education	4.62	1.83	4.15	2.05	1.45	0.15
Participant's education	4.64	1.31	3.93	1.43	3.10	0.00*
Handedness (% right)	95.95		84.29		1.91	0.06
Medication (CPZ equivalents)	-	-	372.53	304.82	-	-
PANSS Positive Symptoms	-	-	14.85	4.76	-	-
PANSS Negative Symptoms	-	-	14.52	4.86	-	-
PANSS General Psychopathology	-	-	29.15	8.38	-	-
PANSS Total Psychopathology	-	-	58.52	13.76	-	-

HCS, healthy comparison subjects; SCZ; patients diagnosed with schizophrenia; PANSS, Positive and Negative Syndrome Scale; M, mean; SD, standard deviation; CPZ, chlorpromazine. Education level for the replication sample was determined based on the following scale: Grade 6 or less = 1; Grade 7–11 = 2; high school graduate = 3; attended college = 4; graduated 2 years college = 5; graduated 4 years college = 6; attended graduate or professional school = 7; Completed graduate or professional school = 8. CPZ equivalents were calculated according to latest validated approaches (Andreasen et al. 2010). * denotes a significant T statistic for the between-group t-test.

Adult Reading (WTAR) depending on the study protocol] (Spreen and Strauss 1998). As in our prior studies, these measures were normed and converted to IQ equivalents for each subject. If more than one premorbid achievement measure was available per subject, the scaled scores were averaged per standard practice (Lezak 1995). Here we did not exclude patients with lifetime co-morbid Axis I anxiety disorders and/or history of substance abuse in the SCZ sample to ensure an inclusive and representative sample of patients (Krystal et al. 2006). However, all discovery sample SCZ participants were required to be abstinent >6 months prior to the study. Healthy comparison subjects (HCS) (N = 90) were recruited through media advertisements and flyers posted in the Medical Center area. Inclusion criteria for HCS were: i) no current or lifetime Axis I psychiatric disorder, as assessed by SCID-NP; ii) no history of medical or neurological conditions; and iii) no history of psychotic disorders in first-degree relatives (reported by detailed family history) (Anticevic et al. 2011; Cole et al. 2011; Anticevic et al. 2012).

The SCZ replication sample (N = 71) was provided to the neuroimaging community by the COBRE initiative. Critically, this large and independent SCZ sample has been extensively characterized, demographically matched to a distinct sample of healthy comparison subjects, and quality-assured across a number of prior reports (http://fcon_1000.projects.nitrc.org/indi/retro/cobre.html). Replication sample SCZ patients were excluded if they had: i) history of neurological disorder; ii) history of mental retardation; ii) history of severe head trauma with more than 5 minutes loss of consciousness; iv) history of substance abuse or dependence within the last 12 months. Diagnostic decisions were reached using the SCID interview for the DSM-IV. Collectively, these criteria and demographics were highly comparable across the two SCZ samples. In both discovery and replication samples, symptoms were assessed using the Positive and Negative Syndrome Scale (PANSS) (Kay et al. 1987) (Table 1-2).

MRI acquisition

Discovery Sample: Structural images were acquired at the Olin Neuropsychiatry Research Center, Hartford, CT, using a Siemens-Allegra 3 T scanner and a T1-weighted, 3D magnetization-prepared rapid gradient-echo (MPRAGE) sequence (TR/TE/TI = 2200/4.13/766 ms, flip angle = 13°, voxel size [isotropic] = .8mm,

image size = 240x320x208 voxels), with axial slices parallel to the anterior commissure - posterior commissure (AC-PC) line. Three SCZ patients were excluded due to insufficient image quality. *Replication sample:* Data were collected by the Mind Research Network at the University of New Mexico using a Siemens Tim-Trio 3 T scanner. Full acquisition details for the SCZ replication sample and corresponding HCS are noted in previous work (Hanlon et al. 2011; Mayer et al. 2012; Stephen et al. 2013). Structural images were acquired using a 6-minute T1-weighted, 3D MPRAGE sequence (TR/TE/TI = 2530/[1.64, 3.5, 5.36, 7.22, 9.08]/900, flip angle = 7°, voxel size [isotropic] = 1 mm, image size = 256x256x176 voxels), with axial slices parallel to the AC-PC line. All of the above parameters were provided via a publicly distributed website (http://fcon_1000.projects.nitrc.org/indi/retro/cobre.html). Four SCZ patients were excluded here due to insufficient MPRAGE image quality.

MRI data preprocessing

All structural images were preprocessed in the VBM8 and DARTEL toolboxes from SPM8 (Kurth et al. 2010). Anatomical images were first segmented into grey matter, white matter, cerebral spinal fluid, bone and soft tissue implemented in VBM8. This segmentation method builds on New Segmentation with the incorporation of a maximum *a posteriori* technique, partial volume estimation, and two de-noising methods. The segmented gray and white matter images were then DARTEL warped to generate a study-specific template in Montreal Neurological Institute (MNI) space to optimize registration across participants (Ashburner 2007). Individual gray matter images were subsequently normalized to this study-specific template using high-dimensional DARTEL normalization (Ashburner 2007). In VBM8, all images were subjected to non-linear modulation that computed the absolute amount of brain tissue for each participant, corrected for individual head size. Images were then smoothed with a 8 mm full width at half maximum Gaussian kernel with the resulting voxel size 1 .5mm^3. In the discovery sample analysis, these preprocessed images were then entered into the seed partial least squares (PLS) structural covariance analysis (detailed below). Estimated total intracranial volume (eTIV) was calculated by taking the sum of the grey matter, white matter, and cerebrospinal fluid volumes derived from non-normalized segmented images. Estimated whole brain volume (eWBV) was calculated as the proportion of the non-normalized grey and white matter volume divided by eTIV. Finally, the mean voxel-wise proportion of grey matter (pGM) relative to the template was calculated for all participants.

Structural covariance network analysis

The preprocessed structural images from the discovery sample were analyzed with structural seed PLS, as implemented previously (PLSgui version 5.07 run on Matlab 2012b, (Krishnan et al. 2011)). Briefly, seed PLS is a data-driven multivariate statistical technique that reveals structural integrity (e.g. volume of grey matter) across the entire brain that correlates with structural integrity in a seed region, computed across subjects. Put differently, the technique reveals gray matter volume across the entire brain that correlates with the gray matter volume of the seed, across subjects and groups. The between-subject correlation matrix of the structural integrity between the seed and all other brain voxels is decomposed into latent variables (LVs) using singular value decomposition that identifies unique patterns of structural correlation. The advantage of seed PLS is that decomposition and associated resampling techniques consider all voxels simultaneously, thus avoiding the problem of multiple statistical comparisons. Because of its ability to identify brain regions with co-varying structural integrity, this technique is methodologically suited to the investigation of large-scale structural covariance networks, as demonstrated by prior work (Spreng and Turner 2013).

Two seed region coordinates with the highest reliability of network membership were selected based on resting-state functional connectivity MRI in 1000 subjects for the fronto-parietal control network (FPCN), salience network (SN), dorsal attention network (DAN), default (mode) network (DMN), and visual network (VN) (Yeo et al. 2011). Motor network (MN) seeds were selected from functionally localized hand and foot regions (Yeo et al. 2011). Seed regions were: for the FPCN, the rostrolateral prefrontal cortex (X = -40, Y = 50, Z = 7) and anterior inferior parietal lobule (X = -43, Y = -50, Z = 46); for the SN, the anterior insula (X = -31, Y = 11, Z = 8) and dorsal anterior cingulate cortex (X = -5, Y = 15, Z = 32); for the DAN, the anterior MT+ (X = -51, Y = -64, Z = -2) and frontal eye fields (X = -22, Y = -8, Z = 54); for the DMN, the posterior inferior parietal lobule (X = -41, Y = -60, Z = 29) and posterior cingulate cortex (X = -7, Y = -52, Z = 26); for the MN, the foot (X = -6, Y = -26, Z = 76) and hand (X = -41, Y = -20, Z = 62) regions; and for the VN, the extrastriate cortex (peripheral field; X = -3, Y = -74, Z = 23) and V1 (peripheral field; X = -16, Y = -74, X = 7) (see Table 3 for list of all network seeds).

For each network, the structural integrity of each seed (i.e. the proportion of grey matter volume) was extracted (centered on the coordinate, with a neighborhood of three voxels, 10.5mm^3 volume) and averaged with the integrity of the other network seed, then correlated across participants with all other brain voxels. PLS was then used to identify patterns of correlation, referred to here as the structural covariance network. The significance of the LVs was determined by 500 non-parametric permutation tests, using resampling without replacement. Robustness and reliability of each voxel's contribution to the LV was provided by a bootstrap that resampled the data 100 times, with replacement, to estimate the standard error of the weight of each voxel on the LV. A bootstrap ratio (BSR), calculated as the ratio of each weight to its standard error, was thresholded to the top 5% of reliable voxels (FPCN BSR ± 9.85; SN BSR ± 11.32; DAN BSR ± 9.02; DMN BSR ± 8.71; MN BSR ± 11.30; VN BSR ± 5.60), equivalent to $p < 1x10^{-4}$ for display purposes and the calculation of subsequent covariance network scores. To further validate the identified structural covariance networks, the spatial similarity with resting-state functional networks (Yeo et al. 2011) was computed. This similarity was quantified by the proportion of voxels in each structural covariance network that overlapped with each of the functional networks.

For each participant, a composite structural covariance network score was calculated, which provides an index of how strongly each participant expresses the pattern identified by the LV. This score is mathematically expressed as the dot product of the grey matter voxel value in each participant's normalized segmented image and the corresponding voxel salience (i.e. weight) in the spatial pattern derived from the thresholded PLS group result image. The resulting value, a single number, reflects the degree to which the singular structural covariance pattern was manifest in the participant's grey matter and provides a measure of the integrity of each individual participant's brain network. The composite scores were used as the primary depen-

Table 3 List of seed regions used to define individual networks

Network	Region	MNI Coordinate		
		x	y	z
Fronto-parietal Control Network	Rostrolateral prefrontal cortex	-40	50	7
	Anterior inferior parietal lobule	-43	-50	46
Salience network	Anterior insula	-31	11	8
	Dorsal anterior cingulate cortex	-5	15	32
Dorsal Attention Network	MT+	-51	-64	-2
	Frontal eye fields	-22	-8	54
Default-mode Network	Posterior inferior parietal lobule	-41	-60	29
	Posterior cingulate cortex	-7	-52	26
Motor Network	Hand region	-6	-26	76
	Foot region	-41	-20	62
Visual Network	Extrastriate cortex	-3	-74	23
	V1	-16	-74	7

dent measures of interest in subsequent multiple analyses of covariance (MANCOVA) to determine network integrity differences between groups.

In order to produce a complete and direct replication, the composite structural covariance network score in the independent replication sample was based on the structural covariance network images from the discovery sample. This score was the dot product of the grey matter voxel value in the replication sample participant's normalized segmented image and the corresponding voxel salience in the spatial pattern derived from the thresholded PLS discovery sample result image. Covariates in the MANCOVA were the demographical variables gender, age, handedness, and education, as well as global scaling factors for the neuroimaging data, including eTIV, eWBV, and pGM. The inclusion of global grey matter measures allows the examination of specific network integrity effects, over and above potential global grey matter differences. In the final combined sample MANCOVA, the additional covariate of study (i.e. discovery vs. replication dataset) was additionally included. We calculated medication levels using chlorpromazine (CPZ) equivalents according to latest validated approaches (Andreasen et al. 2010), which did not correlate with any of the network scores.

Structural covariance analysis with PLS is sensitive to detecting group-wise differences in qualitative patterns of covariance (e.g. (Persson et al. 2014)) In a final analysis, we assessed SCZ and HCS group differences in the pattern of covariance between the seeds regions and the whole brain across the 6 networks.

Results

Alterations in Structural Covariance

As critical validation of the approach, we first assessed the covariance between the seed network regions and whole brain patterns of grey matter in a Voxel-based morphometry (VBM) seed-based PLS analysis. For each analysis, we observed a significant and reliable pattern of structural covariance, consistent with the topology of these intrinsic connectivity networks (Figure 1; Table 4), replicating prior effects using this method (Spreng and Turner 2013). FPCN seed region integrity covaried with contralateral prefrontal and parietal regions, as well as dorsal anterior cingulate and caudate nucleus. SN seed region integrity covaried with extensive dorsal anterior cingulate cortex and contralateral anterior insula. DAN seed region integrity covaried with contralateral frontal eye fields and MT+, as well as the cuneus, pre-supplementary motor area, bilateral superior parietal lobule, anterior insula and thalamus. DMN seed region integrity covaried with extended posterior cingulate cortex, contralateral posterior inferior parietal lobule, medial prefrontal cortex, bilateral lateral temporal cortex, inferior frontal gyrus, and mid-insula. MN seed region integrity covaried with the bilateral motor strip and supplementary motor area, as well as regions of the insula. VN seed region integrity covaried within a massive extent of occipital cortex, terminating at the parietal-occipital fissure. Structural covariance networks also included some smaller clusters outside of the canonical resting-state functional connectivity (RSFC) networks (see Figure 1 and Table 4 for full results). We also computed the spatial overlap between each of the structural covariance networks and well-validated functional networks derived from resting-state functional connectivity (Yeo et al. 2011), shown in Figure 2. While there are some discrepancies between structural and functional networks (see **Discussion**), there is a high degree of correspondence between the two sets of networks, and the proportion of overlap for each structural network is notably highest for the analogous functional network.

Next, we tested the hypothesis that SCZ patients would show structural network integrity alterations relative to HCS. As predicted, we found a significant difference between SCZ patients and HCS in the discovery sample when using the structural covariance network scores. These scores reflect the degree to which the covariance pattern was manifest in each participant's structural image (i.e. integrity of the participant's grey matter weighted by the group structural covariance of the thresholded network map, Wilks' Lambda $F(6,163) = 2.92$, $p < .01$). Composite scores for the FPCN and SN were significantly lower in SCZ than in HCS [$F(1,168) = 6.89$, $p < .01$ and $F(1,168) = 8.55$, $p < .005$, respectively] (Figure 3). Conversely, no differences were observed for the DAN [$F(1,168) = .07$, $p = .789$], DMN [$F(1,168) = .30$ $p = .584$], MN [$F(1,168) = .42$, $p = .517$) or VN [$F(1,168) = 1.57$, $p = .213$].

In the replication SCZ sample, significant differences were again observed in the structural covariance network composite

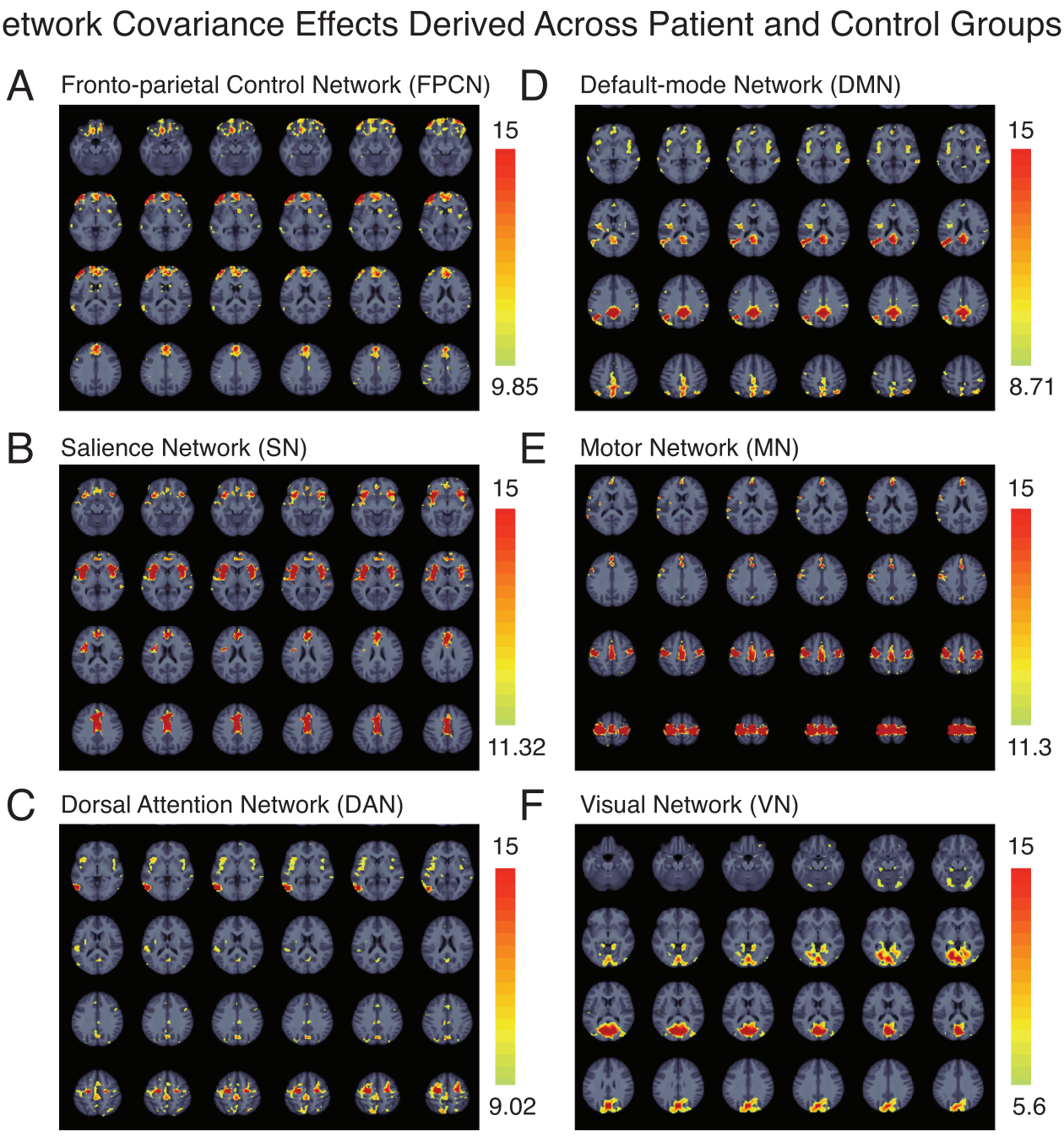

Figure 1. Structural covariance networks. Whole brain structural covariance of the (*A*) fronto-parietal control network (*B*) salience network, (*C*) dorsal attention network, (*D*) default-mode network (*E*) motor network, and (*F*) visual network across all subjects in the Discovery sample (i.e. both patients and healthy comparison subjects). Results are thresholded to the top 5% reliable voxels, all exceeding $p < .001$. PLS is performed in a single analytic step; thus, no correction for multiple comparisons is required (see **Materials and Methods**). The color scale indicates the bootstrap ratio (BSR), equivalent to a z-score.

scores (Wilks' Lambda $F(6,127) = 3.31$, $p < .01$). Consistent with discovery effects, significant decreases were observed for the SCZ group in the FPCN ($F(1,132) = 11.22$, $p < .001$), and the SN ($F(1,132) = 2.87$, $p < .05$, single tailed). Somewhat higher composite scores were observed for the SCZ group in the DAN [$F(1,132) = 7.10$, $p < .01$] and MN ($F(1,132) = 5.29$, $p < .05$). No differences were observed for the DMN [$F(1,132) = .43$ $p = .513$] or VN [$F(1,132) = 1.26$, $p = .263$] in the replication SCZ sample.

We next combined the discovery and replication SCZ samples to achieve maximal power across the two datasets. Significant differences remained in the structural covariance network composite scores [Wilks' Lambda $F(6,303) = 5.32$, $p < .001$). The only significant difference that remained after combining the samples was reduced SCZ integrity of the FPCN [$F(1,308) = 17.63$, $p < .001$, partial $\eta^2 = .054$] and SN [$F(1,308) = 13.90$, $p < .001$, partial $\eta^2 = .043$]. No overall differences were observed in the DAN [$F(1,308) = 1.22$ $p = .271$], DMN [$F(1,308) = .03$ $p = .858$], MN [$F(1,308) = 2.72$, $p = .10$] or VN [$F(1,308) = .18$, $p = .675$] when the samples were combined (see Table 5 for effect sizes of the pair-wise comparisons across structural covariance network scores).

In a final analysis, we assessed whether group-wise differences were observable in the qualitative expression of structural covariance (i.e. was there a significant latent variable that dissociated the groups by the pattern of grey matter covariance). In this analysis, no qualitative differences were observed that separated the groups (all p's > 0.40). This finding suggests that

Table 4 List of regions showing covariance between the seed network regions and whole brain patterns of grey matter

Frontoparietal control network					
Lat	*Region*	*x*	*y*	*z*	*BSR*
L	Rostrolateral prefrontal cortex	−41	51	6	41.98
L	Anterior inferior parietal lobule	−44	−48	48	32.89
R	Dorsal anterior cingulate cortex	2	45	32	16.02
R	Rostrolateral prefrontal cortex	29	63	−6	16.95
R	Anterior insula	45	17	−8	12.94
L	Middle cingulate cortex	0	−17	45	12.51
L	Inferior frontal gyrus	−48	12	29	11.35
R	Lateral temporal cortex	65	−44	11	11.27
R	Anterior inferior parietal lobule	42	−51	54	11.04
L	Caudate nucleus	−9	12	11	10.89
R	Postcentral gyrus	60	−5	39	10.60
Salience network					
Lat	*Region*	*x*	*y*	*z*	*BSR*
L	Anterior insula	−33	9	6	48.30
L	Dorsal anterior cingulate cortex	−3	14	36	34.85
R	Anterior insula	38	23	0	24.48
R	Rostrolateral prefrontal cortex	29	65	−3	15.19
R	Superior temporal gyrus	53	−27	6	13.72
L	Rostrolateral prefrontal cortex	−48	44	−11	13.10
L	Paracentral lobule	−14	−27	72	12.86
L	Middle temporal gyrus	−65	−41	5	12.00
Dorsal attention network					
Lat	*Region*	*x*	*y*	*z*	*BSR*
L	Frontal eye fields	−24	−8	56	31.53
L	Middle temporal motion complex	−51	−66	2	23.45
R	Frontal eye fields	27	−3	57	18.30
L	Cuneus	0	−72	35	13.32
R	Pre-supplementary motor area	6	11	44	12.94
R	Superior parietal lobule	−15	−59	60	12.40
L	Superior parietal lobule	23	−62	63	11.93
L	Anterior insula	−41	15	−3	11.37
R	Anterior insula	38	23	−15	10.66
R	Middle temporal motion complex	54	−71	−2	9.61
L	Thalamus	−14	−30	8	9.89
R	Rostrolateral prefrontal cortex	8	62	0	9.55
Default-mode network					
Lat	*Region*	*x*	*y*	*z*	*BSR*
L	Posterior cingulate cortex	−3	−51	30	34.05
L	Posterior inferior parietal lobule	−44	−63	29	30.74
R	Posterior inferior parietal lobule	39	−62	53	13.35
L	Middle insula	−32	−15	14	12.64
R	Lateral temporal cortex	69	−33	0	12.25
R	Medial prefrontal cortex	2	45	−6	12.12
R	Inferior frontal gyrus	45	17	−5	11.37
L	Lateral temporal cortex	−68	−32	−2	11.29
R	Middle insula	36	0	5	11.28
L	Rostrolateral prefrontal cortex	−41	57	−2	10.57
L	Postcentral gyrus	−48	−11	54	9.88

Continued

Table 4 Continued

Motor network					
Lat	*Region*	x	y	z	*BSR*
L	Motor cortex	−38	−21	66	71.32
R	Motor cortex	29	−26	69	36.31
L	Supplementary motor area	−2	−21	63	29.45
L	Posterior insula	−38	−8	5	16.66
R	Insula	45	17	−6	16.55
L	Rostrolateral prefrontal cortex	−27	63	−2	16.34
L	Lateral temporal cortex	−65	−51	12	14.99
L	Precuneus	−8	−71	60	14.59
R	Thalamus	17	−27	5	13.10
Visual network					
Lat	*Region*	x	y	z	*BSR*
L	Occipital cortex	−14	−72	3	47.51
R	Precentral gyrus	44	−20	63	6.40

Note: BSR – bootstrap ratio equivalent to a z-score

there are no differences in the pattern of structural covariance between the seed regions and the rest of the brain to dissociate SCZ from HCS, and that a single factor structure is more appropriate to account for these data (but see (Winterer et al. 2006) for a discussion of multidimensional functional differences). Only quantitative differences in the integrity of the networks were observed as described above.

Relationship Between Structural Findings and Schizophrenia Symptoms

Finally, we quantified across-subject relationships between structural covariance network scores and SCZ symptoms, measured using PANSS (Kay et al. 1987). Given no strong *a priori* predictions, we comprehensively examined all relationships across networks and symptoms to provide an exploratory guide for future studies (Figure 4), while appropriately accounting for type I error. Two important motifs emerged: i) as evident from the correlation matrix, there were no strong relationships between structural network covariance scores and symptoms (all r-values $<.4$), despite more than adequate statistical power ($N > 150$); ii) patient results revealed consistent and strong across-subject relationships for all structural networks, suggesting that the same patients generally exhibit low (or high) network covariance across networks (Figure 5). Collectively, the lack of symptom relationships and strong across-network relationships suggest a stable 'trait-like' effect.

Discussion

Emerging functional investigations have documented abnormalities across large-scale neural networks in SCZ (Anticevic et al. 2013a; Anticevic et al. 2013b; Uhlhaas 2013). However, it remains unknown if similar alterations occur in the structural integrity of these networks, which could be identified by patterns of structural covariance. To address this gap in knowledge, we characterized the structural covariance of six major networks in SCZ: FPCN, SN, DAN, DMN, MN, and VN. We quantified differences in the grey matter integrity of these networks between a large sample of individuals diagnosed with SCZ ($N = 90$) and HCS ($N = 90$). Next, we fully replicated the identified patterns in an independent large SCZ dataset ($N = 71$). We identified and replicated reliable reductions in the integrity of the FPCN and SN in SCZ. We found highly stable individual differences in the integrity of structural covariance networks across patients. Exploratory symptom analyses, despite being adequately powered, revealed generally weak relationships, suggesting that the integrity of the structural covariance networks may be a 'trait' effect, possibly independent of current clinical status. Collectively, these replicated effects demonstrate that chronic SCZ is associated with widespread and robust structural integrity disruptions across associative cortices (Lefort-Besnard et al. 2018), in line with emerging functional network investigations (Baker et al. 2014; Yang et al. 2014).

Structural Network Integrity Abnormalities are Evident in Chronic Schizophrenia

This study demonstrates that multiple large-scale structural covariance networks are observable using a seed-based PLS approach. This approach allows for an investigation of multivariate patterns in structural network covariance, which can be applied to clinical datasets. This approach is capable of detecting large-scale brain networks by observing inter-individual differences in co-varying brain volume with other brain structures across subjects. While most canonical regions are also apparent with RSFC methods (DuPre and Spreng 2017), subtle differences also emerge that warrant further investigation (e.g. (Clos et al. 2014). For instance, the hippocampal formation is not observed in the current sample or in other default network structural covariance networks (Spreng and Turner 2013), but is reliably involved in RSFC (Vincent et al. 2006). However, some subcortical structures are observed to covary with cortical nodes, such as the caudate with prefrontal and parietal regions of the FPCN. A key strength of the seed PLS method is the derivation of composite structural covariance network scores, which can be used as viable markers of structural alterations across large-scale neural systems concurrently (as opposed to regional changes). These scores reflect the degree to which the covariance pattern in the networks' grey matter was expressed in each participant's brain (i.e., the structural integrity of the identified network). In turn, composite scores can be further quantified in subsequent analyses to examine structural

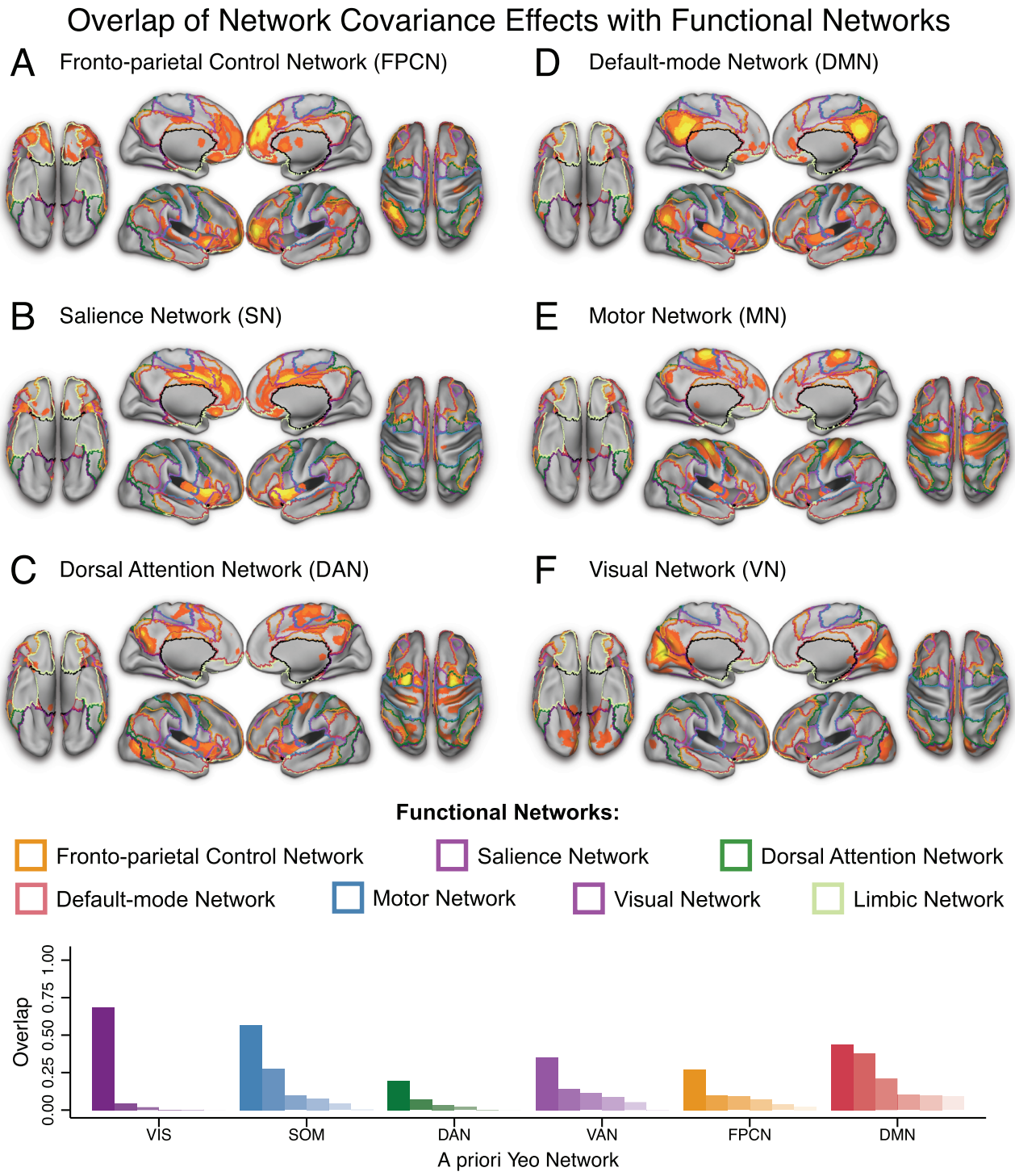

Figure 2. Overlap between structural covariance networks and *a priori* functional networks. Surface views of whole brain structural covariance of the (*A*) fronto-parietal control network (*B*) salience network, (*C*) dorsal attention network, (*D*) default-mode network (*E*) motor network, and (*F*) visual network across all subjects in the Discovery sample (i.e. both patients and healthy comparison subjects). Results are thresholded to the top 5% reliable voxels, all exceeding $p < .001$. PLS is performed in a single analytic step; thus, no correction for multiple comparisons is required (see **Materials and Methods**). The color scale indicates the bootstrap ratio (BSR), equivalent to a *z*-score. (*G*) Proportion of each structural covariance network that overlaps with each of six *a priori* functional networks from (Yeo et al. 2011).

alterations in clinical groups relative to healthy comparison subjects or in relation to symptoms. It should be noted, however, that these scores represent widespread network-level markers. One limitation of the approach is that we cannot localize the specific areas of seed-related covariance disruption; therefore it remains unclear whether the difference is driven by a localized abnormality between two regions, or a more global effect on the identified networks.

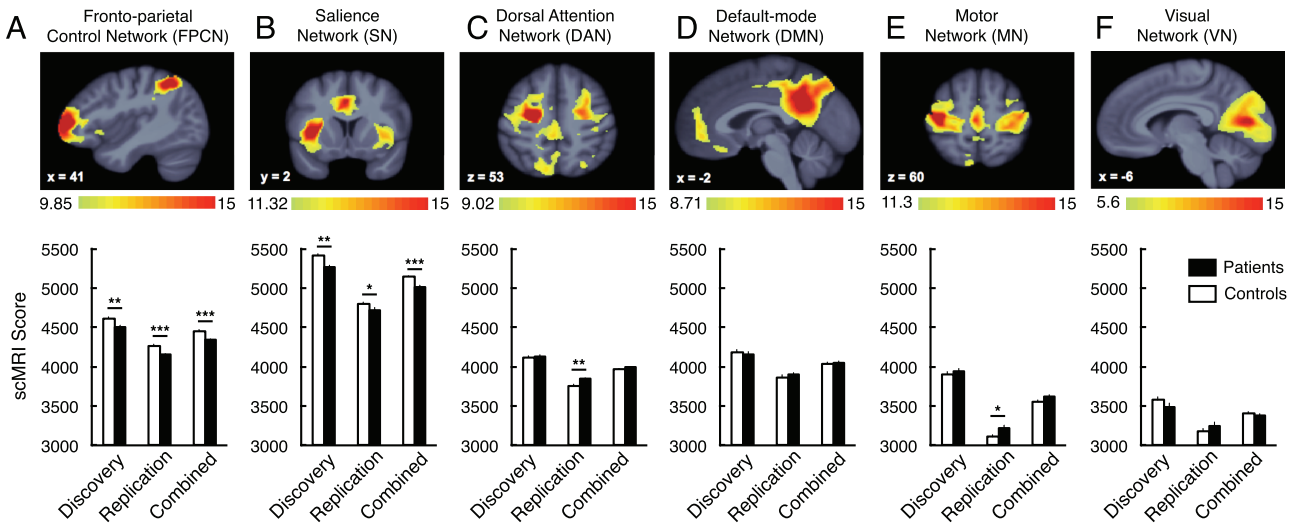

Figure 3. Composite structural covariance network scores group differences. Composite structural covariance network scores are presented for the discovery, replication and combined samples. Structural covariance network topographies were identified in the Discovery sample (see Figure 1 for whole brain results). Whole-brain structural covariance of the (*A*) fronto-parietal control network (*B*) salience network, (*C*) dorsal attention network, (*D*) default-mode network (*E*) motor network, and (*F*) visual network. *p < .05, **p < .01, ***p < .001. Error bars denote +/− 1 standard error of the mean. The color scale indicates the bootstrap ratio (BSR), equivalent to a z-score.

Table 5 Effect Sizes for pair-wise comparisons across structural covariance network scores

	Statistic	Discovery	Replication	Combined
Fronto-parietal Control Network	t Value	2.63	3.35	4.20
	P Value	0.009*	0.001*	0.000035*
	Cohen's d	0.40	0.57	0.47
Salience Network	t Value	2.92	1.69	3.73
	P Value	0.004*	0.093	0.00023*
	Cohen's d	0.44	0.29	0.42
Dorsal Attention Network	t Value	0.27	2.67	1.11
	P Value	0.789	0.009*	0.271
	Cohen's d	0.04	0.45	0.12
Default-Mode Network	t Value	0.55	0.66	0.17
	P Value	0.584	0.513	0.858
	Cohen's d	0.08	0.11	0.02
Motor Network	t Value	0.65	2.30	1.65
	P Value	0.517	0.023*	0.1
	Cohen's d	0.10	0.39	0.19
Visual Network	t Value	1.25	1.12	0.42
	P Value	0.213	0.263	0.675
	Cohen's d	0.19	0.19	0.05

Many SCZ studies have documented regional structural alterations (Pearlson and Marsh 1999; Pearlson and Calhoun 2007; Ellison-Wright et al. 2014). However, wide-spread structural alterations in complex psychiatric disease likely do not occur independently within specific cortical location, but rather may follow spatially coherent patterns that cluster around common trajectories. This pattern has been reported in early development (Zielinski et al. 2010; Alexander-Bloch et al. 2013a; Khundrakpam et al. 2013), as well as in age-related decline and dementia (Chen et al. 2011; Zhu et al. 2012; Spreng and Turner 2013). Recent work suggests that the distributed structural covariance pattern is mediated in part by cortical gene expression (Romero-Garcia et al. 2018; Yee Y et al. 2018). Disturbances in structural covariance patterns in SCZ have been associated with the expression profiles of the genes involved in therapeutic targets and brain development (Liu et al. 2018). A corollary of this observation is that in SCZ, we might observe similar 'co-varying' alterations in structure across areas that form functional systems, such as the FPCN (Fornito et al. 2012; Fornito et al. 2013), perhaps reflecting an underlying pathophysiological mechanism (Schobel et al. 2013). Such distributed changes in structural covariance would imply that SCZ is associated with significantly reduced hierarchy with increased connection distance across functionally related cortical regions

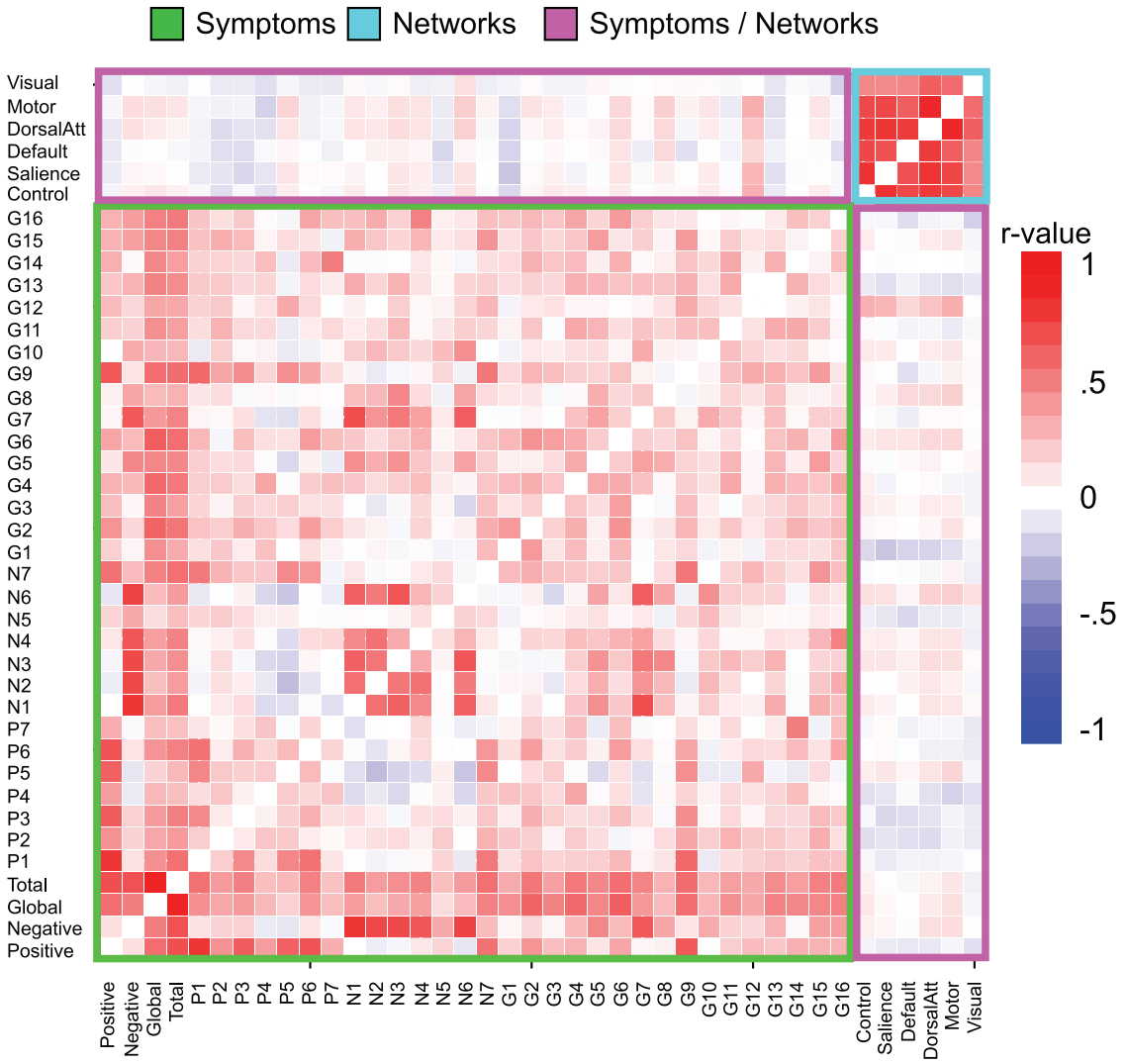

Figure 4. Relationship between structural covariance network scores and symptoms. Comprehensive individual difference analysis presented in correlation matrix form across all symptoms (green box), structural covariance networks (cyan box), and the relationship between networks and symptoms (pink box). As evident from individual correlation values, these exploratory analyses indicated that there were generally no strong relationships between symptoms and covariance network scores, suggesting a 'trait' effect. In contrast, the magnitude of covariance across patients in one network correlated highly with covariance across all other networks (cyan box in the upper right corner. For completeness, we present scatterplots (see Figure 4) to ensure that outliers are not driving these network relationships.

(Bassett et al. 2008). Two regions in particular, the middle frontal gyrus and anterior insula - key nodes of the FPCN and SN, respectively - have been associated with reduced connectivity in SCZ (Palaniyappan et al. 2013). Furthermore, recent resting-state functional network studies have identified widespread signal disruptions in associative cortices in SCZ (Baker et al. 2014; Yang et al. 2014). Present findings highlight the possibility that structural brain differences, measured at the level of whole-brain network integrity, are similarly affected in SCZ, providing a convergent multi-modal neuroimaging marker that could be leveraged in future structure–function studies (c.f. (Lefort-Besnard et al. 2018)).

Structural Network Integrity Abnormalities are Preferentially Found in Associative Cortices

Consistent with predictions, we identified robust alterations in the FPCN and the SN. Both neural networks have been repeatedly implicated in chronic SCZ via task-based activation studies and resting-state functional investigations (Repovs et al. 2011; Barch and Ceaser 2012; Repovs and Barch 2012; Palaniyappan et al. 2013; Baker et al. 2014; Yang et al. 2014). Thus, present findings provide converging support for concurrent structural network alterations in higher-order associative cortices (Palaniyappan et al. 2015; Lefort-Besnard et al. 2018; Palaniyappan et al. 2018). SCZ patients across both samples exhibited coherent and highly co-varying reductions across voxels that are part of wider neural systems. This finding in part challenges the possibility that only 'localized', independent structural changes occur in SCZ. Instead, this effect is more consistent with the hypothesis that SCZ is associated with co-occurring structural alterations within distributed systems – a hypothesis that is further supported by robust individual difference effects (see Figure 5). As noted, these alterations were most apparent for higher-order FPCN and SN (see also, (Palaniyappan et al. 2015; Palaniyappan et al. 2018)) and were

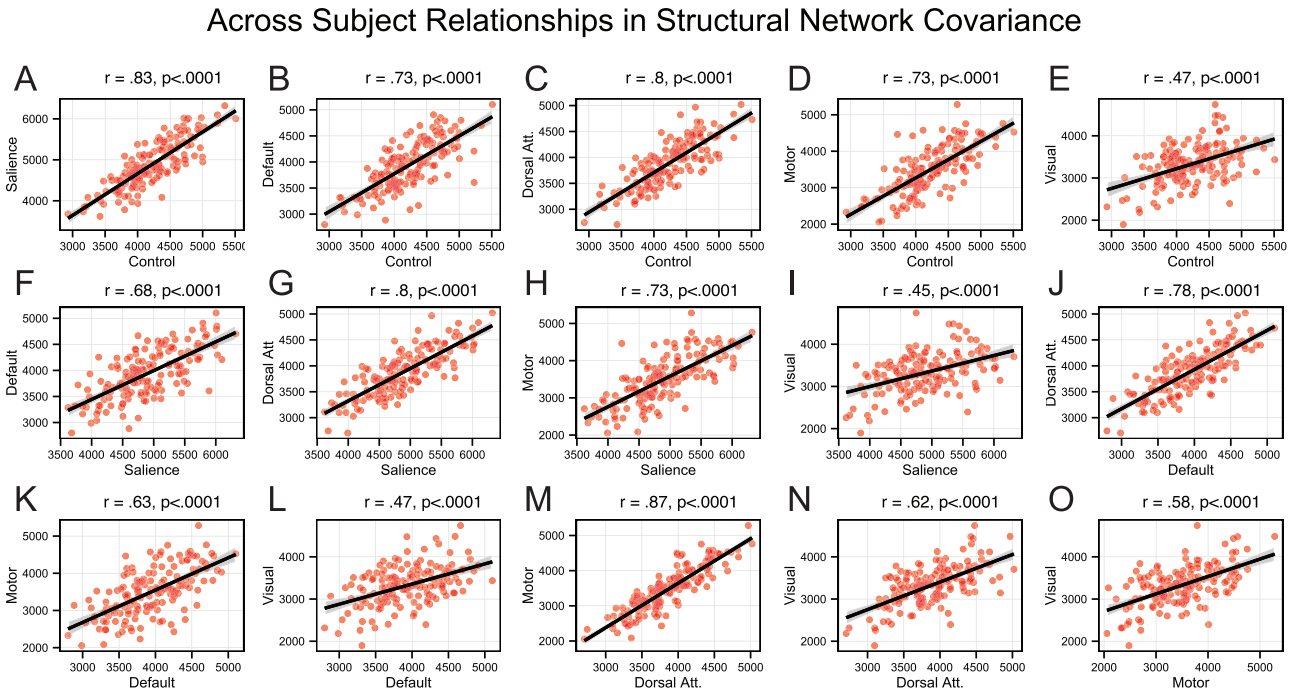

Figure 5. Relationship across covariance networks. (*A*–*O*) Scatterplots showing across-subject relationships for patients (N = 154) between structural network covariance for all networks. As evident from scatterplots, outliers did not drive these network relationships. These highly significant effects indicate that the magnitude of structural integrity across networks was linearly related across patients. All relationships survived highly stringent Bonferroni correction.

not replicated in lower-order motor and visual systems. This dissociation is compelling, as some studies have clearly documented functional alterations in primary sensory systems using task-evoked paradigms (Yoon et al. 2010). Relatedly, it has been established that sensory systems in SCZ show profound alterations with thalamo-cortical networks defined both functionally (Woodward et al. 2012; Anticevic et al. 2013a; Anticevic et al. 2014) and structurally (Mitelman et al. 2006). However, preferential structural alterations in higher-order associative cortices could reflect two possibilities: i) there may exist more subtle alterations in primary sensory systems, which we were not powered enough to observe (although this is unlikely given the size of current samples); ii) there may be an underlying neurobiological mechanism that is 'driving' more rapid or profound structural disturbances in some higher-order associative networks; this may relate to unique computational mechanisms in higher-order associative cortical territories (Murray et al. 2014). The combination of pre-clinical and computational studies that link mechanistic pharmacological probes to patterns of altered structure may help address this question (see below). It is unclear whether these specific structural patterns emerge only as a consequence of long-standing illness, although recent evidence suggests observable difference in individuals at ultra-high risk for psychosis across multiple structural covariance networks, including the executive and salience (Heinze et al. 2015).

Structural Network Integrity is Highly Consistent Across Subjects but Unrelated to Current Schizophrenia Symptoms

We attempted several exploratory individual difference analyses, which revealed two general patterns: i) there were no apparent strong relationships between network covariance effects and current SCZ symptoms; ii) conversely, we identified consistent and highly robust relationships in structural covariance network scores across patients for each of the identified networks, suggesting a consistent effect across subjects. Put differently, patients with the most structural integrity 'degradation' in one network exhibited structural integrity 'degradation' across other networks, suggesting a robust and consistent brain-wide pattern across subjects. The combination of these two effects suggests that the identified structural covariance network effects are perhaps indicative of a 'trait' marker, which is generally unrelated to clinical status at the time of the scan. However, as noted above, it remains unknown whether these network-level measures show 'state-like' alterations along the illness course. Furthermore, impaired performance on a variety of neuropsychological tests can stably differentiate patients with schizophrenia from unaffected controls (Saykin et al. 1994; Rund 1998; Nuechterlein et al. 2004) and previous studies have reported correlations between cortical thickness and neuropsychological functioning in schizophrenia (Gur et al. 2000; Hartberg et al. 2010; Ehrlich et al. 2012). However, precise measures of cognitive (dys)function, which may be linked to observed structural covariance alterations, were not available in the current study.

Putative Mechanisms of Altered Structural Network Co-variance

Developmental changes in regional brain volumes have been frequently reported (Thompson et al. 2005). Emerging evidence suggests that such changes are not isolated within specific brain regions, but rather occur in topographically coherent patterns across the brain. Zielinski and colleagues demonstrated that

structural covariance across spatially distributed brain regions follows a specific developmental trajectory from childhood to early adulthood (Zielinski et al. 2010). These structural changes continue across the lifespan, with significant differences in the topography and architecture of large-scale networks observed between younger and older healthy adults (Mitelman et al. 2006; Khundrakpam et al. 2013; Di et al. 2017). Indirect evidence suggests that the brain's functional architecture may provide a common pathway for structural brain changes across development, whereby structural covariance and intrinsic connectivity networks are coupled in healthy young adults. Interestingly, patterns of brain atrophy in neurodegenerative syndromes also cohere with large-scale functional network topographies (Seeley et al. 2009).

Collectively, these findings suggest that examining structural covariance in regions with known intrinsic functional connectivity may be a sensitive marker of shared structural integrity change. Therefore, structural measures of network integrity appear sensitive to widespread alterations in connectivity across an entire neural system. A key hypothesis for future studies is whether system-wide structural alterations involve time-dependent changes that are exacerbated over the course of the illness. For instance, recent animal studies have mechanistically linked repeated actuate dosing of N-methyl-D-aspartate receptor antagonists in hippocampal circuits to subsequent structural decline (Schobel et al. 2013). The present study provides a system-level structural neural marker, which may prove more sensitive to such time-dependent alterations. Also, examining these structural changes cross-diagnostically (Anticevic et al. 2013a; Anticevic et al. 2014; Yang et al. 2014) and during early illness phases (Anticevic et al. 2013c), as done in functional studies, will be necessary to address questions concerning long-term medication effects. Lastly, to improve understanding of these system-wide effects, future studies should explicitly combine neuroimaging modalities in order to determine whether structural and functional network effects are linked (Sui et al. 2012). Combining such measures across modalities may substantially improve neuro-diagnostic tools that could guide better classification and treatment approaches (Sui et al. 2012).

Limitations

Several limitations need to be considered. First, as noted, it is impossible to fully rule out the possibility that present effects are a consequence of long-term medication (although CPZ equivalents did not correlate with reported findings). As noted, illness duration may have also played a role in these effects. It remains unclear whether the observed effects predate illness onset and/or occur in association with initial symptoms, or whether they only present as a consequence of longer-standing illness. Although we failed to observe significant relationships with symptoms, it remains unknown whether these effects are indeed specific to SCZ or whether they are more generally associated with severe mental illness, a possibility that can be examined in future cross-diagnostic studies. Another consideration relates to the quality of structural images. Future studies that capitalize on improving scan quality (e.g. by leveraging the innovations made available via the Human Connectome Project (Glasser et al. 2013) may yield more sensitive effects. Finally, while we did not find strong relationships with symptoms, we did not have access to state-of-the-art measures of higher-order cognitive performance (e.g. working memory and executive functioning) in these samples (Barch and Ceaser 2012). It is possible that structural network integrity degradation, especially in the FPCN, relates to cognitive deficits, and this possibility should be systematically examined in future SCZ studies.

Conclusion

We identified and replicated consistent and robust structural network disruptions in two large chronic SCZ samples. We found preferential reduction in the structural integrity of the FPCN and SN in SCZ, which were consistent across samples and highly related across patients. The lack of symptom effects suggests that altered structural covariance network integrity may be a 'trait-like' effect, possibly independent of current clinical symptom severity. Collectively, these replicated effects provide a novel index of structural network alteration in chronic SCZ that can be readily combined with additional neuroimaging modalities, perhaps yielding more sensitive neural markers for SCZ.

Notes

A.A. and J.D.M. consult for BlackThorn Therapeutics, and A.A. is a member of its scientific advisory board.

Funding

This work was supported in part by a grant from the Canadian Institutes of Health Research to R.N.S., a Research Scholar supported by the Fonds de recherche du Québec - Santé as well as National Institute of Mental Health (NIMH) grants 5R01MH112189 and 5R01MH108590 to A.A.

References

Alexander-Bloch A, Giedd JN, Bullmore E. 2013a. Imaging structural co-variance between human brain regions. *Nature reviews Neuroscience*. 14:322–336.

Alexander-Bloch AF, Vertes PE, Stidd R, Lalonde F, Clasen L, Rapoport J, Giedd J, Bullmore ET, Gogtay N. 2013b. The anatomical distance of functional connections predicts brain network topology in health and schizophrenia. *Cereb Cortex*. 23:127–138.

Andreasen NC, Pressler M, Nopoulos P, Miller D, Ho B-C. 2010. Antipsychotic dose equivalents and dose-years: A standardized method for comparing exposure to different drugs. *Biological psychiatry*. 67:255–262.

Anticevic A, Brumbaugh MS, Winkler AM, Lombardo LE, Barrett J, Corlett PR, Kober H, Gruber J, Repovs G, Cole MW, Krystal JH, Pearlson GD, Glahn DC. 2012. Global prefrontal and Fronto-amygdala Dysconnectivity in bipolar I disorder with psychosis history. *Biological Psychiatry*. 73: 565–573.

Anticevic A, Cole MW, Repovs G, Murray JD, Brumbaugh MS, Winkler AM, Savic A, Krystal JH, Pearlson GD, Glahn DC. 2013a. Characterizing Thalamo-cortical disturbances in schizophrenia and bipolar illness. *Cereb Cortex [Epub]*. 24: 3116–3130.

Anticevic A, Cole MW, Repovs G, Savic A, Driesen NR, Yang G, Cho YT, Murray JD, Glahn DC, Wang X-J, Krystal JH. 2013b. Connectivity, pharmacology, and computation: Toward a mechanistic understanding of neural system dysfunction in schizophrenia. *Frontiers in Psychiatry*. 4:169.

Anticevic A, Repovs G, Corlett PR, Barch DM. 2011. Negative and non-emotional interference with visual working memory in schizophrenia. *Biological Psychiatry*. 70:1159–1168.

Anticevic A, Tang Y, Cho YT, Repovs G, Cole MW, Savic A, Wang F, Krystal JH, Xu K. 2013c. *Amygdala Connectivity Differs Among Chronic, Early Course, and Individuals at Risk for Developing Schizophrenia*. *Schizophr Bull* [Epub ahead of print]. 40:1105–1116.

Anticevic A, Yang G, Savic A, Murray JD, Cole MW, Repovs G, Pearlson GD, Glahn DC. 2014. Medio-dorsal and visual thalamic connectivity differ in schizophrenia and bipolar disorder with and without psychosis history. *Schizophr Bull [Epub]*. 40:1227–1243.

Ashburner J. 2007. A fast Diffeomorphic image registration algorithm. *Neuroimage*. 38:95–113.

Baker JT, Holmes AJ, Masters GA, Yeo BT, Krienen F, Buckner RL, Ongür D. 2014. Disruption of cortical association networks in schizophrenia and psychotic bipolar disorder. *JAMA Psychiatry*. 72:109–118.

Barch DM, Ceaser A. 2012. Cognition in schizophrenia: Core psychological and neural mechanisms. *Trends In Cognitive Sciences*. 16:27–34.

Bassett DS, Bullmore E, Verchinski BA, Mattay VS, Weinberger DR, Meyer-Lindenberg A. 2008. Hierarchical organization of human cortical networks in health and schizophrenia. *J Neurosci*. 28:9239–9248.

Bora E, Fornito A, Radua J, Walterfang M, Seal M, Wood SJ, Yücel M, Velakoulis D, Pantelis C. 2011. Neuroanatomical abnormalities in schizophrenia: A multimodal voxelwise meta-analysis and meta-regression analysis. *Schizophrenia Research*. 127:46–57.

Buckner RL, Krienen FM, Yeo BT. 2013. Opportunities and limitations of intrinsic functional connectivity MRI. *Nature Neuroscience*. 16:832–837.

Chen ZJ, He Y, Rosa-Neto P, Gong G, Evans AC. 2011. Age-related alterations in the modular organization of structural cortical network by using cortical thickness from MRI. *Neuroimage*. 56:235–245.

Clos M, Rottschy C, Laird AR, Fox PT, Eickhoff SB. 2014. Comparison of structural covariance with functional connectivity approaches exemplified by an investigation of the left anterior insula. *Neuroimage*. 99:269–280.

Cocchi L, Harding IH, Lord A, Pantelis C, Yücel M, Zalesky A. 2014. Disruption of structure–function coupling in the schizophrenia connectome. *NeuroImage Clinical*. 4:779–787.

Cole MW, Anticevic A, Repovs G, Barch DM. 2011. Variable global dysconnectivity and individual differences in schizophrenia. *Biological Psychiatry*. 70:43–50.

Coyle JT. 2006. Glutamate and schizophrenia: Beyond the dopamine hypothesis. *Cell Mol Neurobiol*. 26:365–384.

Di X, Gohel S, Thielcke A, Wehrl HF, Biswal BB. Alzheimer's disease neuroimaging I. 2017. Do all roads lead to Rome? A comparison of brain networks derived from inter-subject volumetric and metabolic covariance and moment-to-moment hemodynamic correlations in old individuals. *Brain Struct Funct*. 222:3833–3845.

DuPre E, Spreng RN. 2017. Structural covariance networks across the life span, from 6 to 94 years of age. *Netw Neurosci*. 1:302–323.

Ehrlich S, Brauns S, Yendiki A, Ho BC, Calhoun V, Schulz SC, Gollub RL, Sponheim SR. 2012. Associations of cortical thickness and cognition in patients with schizophrenia and healthy controls. *Schizophr Bull*. 38:1050–1062.

Ellison-Wright I, Nathan PJ, Bullmore ET, Zaman R, Dudas RB, Agius M, Fernandez-Egea E, Muller U, Dodds CM, Forde NJ, Scanlon C, Leemans A, McDonald C, Cannon DM. 2014. Distribution of tract deficits in schizophrenia. *BMC psychiatry*. 14:99.

First MB, Spitzer RL, Miriam G, Williams JBW. 2002. *Structured clinical interview for DSM-IV-TR Axis I Disorders, Research Version, Non-patient Edition (SCID-I/NP)*. New York: Biometrics Research, New York State Psychiatric Institute.

Fornito A, Zalesky A, Breakspear M. 2013. Graph analysis of the human connectome: Promise, progress, and pitfalls. *Neuroimage*. Epub ahead of print. 80:426–444.

Fornito A, Zalesky A, Pantelis C, Bullmore ET. 2012. Schizophrenia, neuroimaging and connectomics. *Neuroimage*. 62:2296–2314.

Frangou S. 2014. A systems neuroscience perspective of schizophrenia and bipolar disorder. *Schizophrenia bulletin*. 40:523–531.

Glasser MF, Sotiropoulos SN, Wilson JA, Coalson TS. 2013. The minimal preprocessing pipelines for the human Connectome project. *Neuroimage*. 80:105–124.

Gur RE, Cowell PE, Latshaw A, Turetsky BI, Grossman RI, Arnold SE, Bilker WB, Gur RC. 2000. Reduced dorsal and orbital prefrontal gray matter volumes in schizophrenia. *Archives of General Psychiatry*. 57:761–768.

Hanlon FM, Houck JM, Pyeatt CJ, Lundy SL, Euler MJ, Weisend MP, Thoma RJ, Bustillo JR, Miller GA, Tesche CD. 2011. Bilateral hippocampal dysfunction in schizophrenia. *NeuroImage*. 58:1158–1168.

Hartberg CB, Lawyer G, Nyman H, Jonsson EG, Haukvik UK, Saetre P, Bjerkan PS, Andreassen OA, Hall H, Agartz I. 2010. Investigating relationships between cortical thickness and cognitive performance in patients with schizophrenia and healthy adults. *Psychiatry Res*. 182:123–133.

Heinze K, Reniers RL, Nelson B, Yung AR, Lin A, Harrison BJ, Pantelis C, Velakoulis D, McGorry PD, Wood SJ. 2015. Discrete alterations of brain network structural covariance in individuals at ultra-high risk for psychosis. *Biol Psychiatry*. 77: 989–996.

Kay SR, Fiszbein A, Opler LA. 1987. The positive and negative syndrome scale (PANSS) for schizophrenia. *Schizophrenia Bulletin*. 13:261–276.

Khundrakpam BS, Reid A, Brauer J, Carbonell F, Lewis J, Ameis S, Karama S, Lee J, Chen Z, Das S, Evans AC, Brain Development Cooperative G. 2013. Developmental changes in organization of structural brain networks. *Cereb Cortex*. 23:2072–2085.

Krishnan A, Williams LJ, McIntosh AR, Abdi H. 2011. Partial least squares (PLS) methods for neuroimaging: A tutorial and review. *Neuroimage*. 56:455–475.

Krystal JH, D'Souza DC, Gallinat J, Driesen NR, Abi-Dargham A, Petrakis I, Heinz A, Pearlson GD. 2006. The vulnerability to alcohol and substance abuse in individuals diagnosed with schizophrenia. *Neurotoxicity Research*. 10: 235–252.

Kuang C, Buchy L, Barbato M, Makowski C, MacMaster FP, Bray S, Deighton S, Addington J. 2017. A pilot study of cognitive insight and structural covariance in first-episode psychosis. *Schizophr Res*. 179:91–96.

Kurth F, Luders E, Gaser C. 2010. *VBM8 toolbox manual*, http://www.neuro.uni-jena.de/vbm/.

Lefort-Besnard J, Bassett DS, Smallwood J, Margulies DS, Derntl B, Gruber O, Aleman A, Jardri R, Varoquaux G, Thirion B, Eickhoff SB, Bzdok D. 2018. Different shades of

default mode disturbance in schizophrenia: Subnodal covariance estimation in structure and function. *Hum Brain Mapp*. 39:644–661.

Lezak MD. 1995. *Neuropsychological Assessment*. New York: Oxford University Press

Liu F, Tian H, Li J, Li S, Zhuo C. 2018. Altered voxel-wise gray matter structural brain networks in schizophrenia: Association with brain genetic expression pattern. *Brain Imaging Behav*. in press (doi: 10.1007/s11682-018-9880-6)

Lynn CW, Bassett DS. 2018. The physics of brain network structure, function, and control. *Reviews Physics* in press DOI: https://doi.org/10.1038/s42254-019-0040-8.

Mayer AR, Ruhl D, Merideth F, Ling J, Hanlon FM, Bustillo J, Cañive J. 2012. Functional imaging of the hemodynamic sensory gating response in schizophrenia. *Human Brain Mapping*. 34:2302–2312.

Mitelman SA, Byne W, Kemether EM, Hazlett EA, Buchsbaum MS. 2006. Correlations between volumes of the pulvinar, centromedian, and mediodorsal nuclei and cortical Brodmann's areas in schizophrenia. *Neurosci Lett*. 392:16–21.

Murray CJL, Lopez AD. 1996. *The global burden of disease: a comprehensive assessment of mortality and disability from diseases, injuries and risk factors in 1990 and projected to 2020*. Cambridge: Harvard University Press

Murray CJL, Lopez AD, Harvard School of Public Health., World Health Organization., World Bank. 1996. *The global burden of disease : a comprehensive assessment of mortality and disability from diseases, injuries, and risk factors in 1990 and projected to*. Cambridge, MA: Published by the Harvard School of Public Health on behalf of the World Health Organization and the World Bank ; Distributed by Harvard University Press, p. 2020

Murray JD, Bernacchia A, Freedman DJ, Romo R, Wallis JD, Cai X, Padoa-Schioppa C, Pasternak T, Seo H, Lee D, Wang X-J. 2014. A hierarchy of intrinsic timescales across primate cortex. *Nature Neuroscience*. E-pub ahead of print. 17:1661–1663.

Nuechterlein KH, Barch DM, Gold JM, Goldberg TE, Green MF, Heaton RK. 2004. Identification of separable cognitive factors in schizophrenia. *Schizophrenia Research*. 72:29–39.

Palaniyappan L, Hodgson O, Balain V, Iwabuchi S, Gowland P, Liddle P. 2019. Structural covariance and cortical reorganisation in schizophrenia: A MRI-based morphometric study. *Psychol Med*. 49:412–420. doi: 10.1017/S0033291718001010.

Palaniyappan L, Park B, Balain V, Dangi R, Liddle P. 2015. Abnormalities in structural covariance of cortical gyrification in schizophrenia. *Brain Struct Funct*. 220:2059–2071.

Palaniyappan L, Simmonite M, White TP, Liddle EB, Liddle PF. 2013. Neural primacy of the salience processing system in schizophrenia. *Neuron*. 79:814–828.

Pearlson GD, Calhoun V. 2007. Structural and functional magnetic resonance imaging in psychiatric disorders. *Canadian journal of psychiatry Revue canadienne de psychiatrie*. 52:158–166.

Pearlson GD, Marsh L. 1999. Structural brain imaging in schizophrenia: A selective review. *Biological Psychiatry*. 46: 627–649.

Pearlson GD, Petty RG, Ross CA, Tien AY. 1996. Schizophrenia: A disease of heteromodal association cortex. *Neuropsychopharmacology*. 14:1–17.

Persson J, Spreng RN, Turner GR, Herlitz A, Morell A, Stening E, Wahlund L-O, Wikström J, Söderlund H. 2014. Sex differences in volume and structural covariance of the anterior and posterior hippocampus. *NeuroImage*. 99:215–225.

Power JD, Cohen AL, Nelson SM, Wig GS, Barnes KA, Church JA, Vogel AC, Laumann TO, Miezin FM, Schlaggar BL, Petersen SE. 2011. Functional network organization of the human brain. *Neuron*. 72:665–678.

Repovs G, Barch DM. 2012. Working memory related brain network connectivity in individuals with schizophrenia and their siblings. *Frontiers in Human Neuroscience*. 6:137.

Repovs G, Csernansky JG, Barch DM. 2011. Brain network connectivity in individuals with schizophrenia and their siblings. *Biological Psychiatry*. 15:967–973.

Romero-Garcia R, Whitaker KJ, Vasa F, Seidlitz J, Shinn M, Fonagy P, Dolan RJ, Jones PB, Goodyer IM, Consortium N, Bullmore ET, Vertes PE. 2018. Structural covariance networks are coupled to expression of genes enriched in supragranular layers of the human cortex. *Neuroimage*. 171: 256–267.

Rund BR. 1998. A review of longitudinal studies of cognitive functions in schizophrenia patients. *Schizophr Bull*. 24:425–435.

Saykin AJ, Shtasel DL, Gur RE, Kester DB, Mozley LH, Stafiniak P, Gur RC. 1994. Neuropsychological deficits in neuroleptic naive patients with first-episode schizophrenia. *Arch Gen Psychiatry*. 51:124–131.

Schobel SA, Chaudhury NH, Khan UA, Paniagua B, Styner MA, Asllani I, Inbar BP, Corcoran CM, Lieberman JA, Moore H, Small SA. 2013. Imaging patients with psychosis and a mouse model establishes a spreading pattern of hippocampal dysfunction and implicates glutamate as a driver. *Neuron*. 10:81–93.

Seeley WW, Crawford RK, Zhou J, Miller BL, Greicius MD. 2009. Neurodegenerative diseases target large-scale human brain networks. *Neuron*. 62:42–52.

Spreen O, Strauss E. 1998. *A compendium of neuropsychological tests: Administration, norms, and commentary*. New York: Oxford University Press

Spreng RN, Turner GR. 2013. Structural covariance of the default network in healthy and pathological aging. *J Neurosci*. 33:15226–15234.

Stephan KE, Baldeweg T, Friston KJ. 2006. Synaptic plasticity and dysconnection in schizophrenia. *Biological Psychiatry*. 59:929–939.

Stephen JM, Coffman BA, Jung RE, Bustillo JR, Aine CJ, Calhoun VD. 2013. Using joint ICA to link function and structure using MEG and DTI in schizophrenia. *Neuroimage*. 83:418–430.

Sui J, Yu Q, He H, Pearlson GD, Calhoun VC. 2012. A selective review of multimodal fusion methods in schizophrenia. *Frontiers in Human Neuroscience*. 6:27.

Thompson PM, Sowell ER, Gogtay N, Giedd JN, Vidal CN, Hayashi KM, Leow A, Nicolson R, Rapoport JL, Toga AW. 2005. Structural MRI and brain development. *Int Rev Neurobiol*. 67:285–323.

Uhlhaas PJ. 2013. Dysconnectivity, large-scale networks and neuronal dynamics in schizophrenia. *Current Opinion in Neurobiology*. 23:283–290.

Vincent JL, Snyder AZ, Fox MD, Shannon BJ, Andrews JR, Raichle ME, Buckner RL. 2006. Coherent spontaneous activity identifies a hippocampal-parietal memory network. *J Neurophysiol*. 96:3517–3531.

Whitfield-Gabrieli S, Thermenos H, Milanovic S, Tsuang M, Faraone S, McCarley R, Shenton M, Green A, Nieto-Castanon A, Laviolette P, Wojcik J, Gabrieli J, Seidman L. 2009. Hyperactivity and hyperconnectivity of the default network in

schizophrenia and in first-degree relatives of persons with schizophrenia. *Proceedings of the National Academy of Science USA*. 106:1279–1284.

Winterer G, Musso F, Beckmann CF, Mattay V, Egan MF, Jones DW, Callicott JH, Coppola R, Weinberger DR. 2006. Instability of prefrontal signal processing in schizophrenia. *American Journal of Psychiatry*. 163:1960–1968.

Woodward ND, Karbasforoushan H, Heckers S. 2012. Thalamocortical dysconnectivity in schizophrenia. *Am J Psychiatry*. 169:1092–1099.

Yang GJ, Murray JD, Repovs G, Cole MW, Savic A. 2014. M.F. G, Pittenger C, Krystal JH, Wang X-J, Pearlson GD, Glahn DC, Anticevic a. *Altered Global Brain Signal in Schizophrenia*. *Proceedings of the National Academy of Science USA*. 111:7438–7443.

Yee Y, Fernandes DJ, French L, Ellegood J, Cahill LS, Vousden DA, Spencer Noakes L, Scholz J, van Eede MC, Nieman BJ, Sled JG, Lerch JP. 2018. Structural covariance of brain region volumes is associated with both structural connectivity and transcriptomic similarity. *Neuroimage* 179:357–372.

Yeo BT, Krienen FM, Sepulcre J, Sabuncu MR, Lashkari D, Hollinshead M, Roffman JL, Smoller JW, Zollei L, Polimeni JR, Fischl B, Liu H, Buckner RL. 2011. The organization of the human cerebral cortex estimated by intrinsic functional connectivity. *J Neurophysiol*. 106:1125–1165.

Yoon JH, Maddock RJ, Rokem A, Silver MA, Minzenberg MJ, Ragland JD, Carter CS. 2010. GABA concentration is reduced in visual cortex in schizophrenia and correlates with orientation-specific surround suppression. *J Neurosci*. 30:3777–3781.

Zhu W, Wen W, He Y, Xia A, Anstey KJ, Sachdev P. 2012. Changing topological patterns in normal aging using large-scale structural networks. *Neurobiology of Aging*. 33:899–913.

Zielinski BA, Gennatas ED, Zhou J, Seeley WW. 2010. Network-level structural covariance in the developing brain. *Proc Natl Acad Sci U S A*. 107:18191–18196.

Zugman A, Assuncao I, Vieira G, Gadelha A, White TP, Oliveira PP, Noto C, Crossley N, McGuire P, Cordeiro Q, Belangero SI, Bressan RA, Jackowski AP, Sato JR. 2015. Structural covariance in schizophrenia and first-episode psychosis: An approach based on graph analysis. *J Psychiatr Res*. 71:89–96.